Chapter 2
SAR Ground Moving Target Indication and Imaging Theory

Abstract This chapter mainly introduces the basic principles of SAR imaging, signal model, GMTI and GMTIm algorithms. The geometries of stationary and moving targets are established, and the characters of their echoes are analyzed. Based on the analysis, three classical single-channel GMTI algorithms are introduced in this chapter, and their limitations are discussed. Moreover, the principle of GMTIm algorithms with Keystone transform and time-frequency analysis algorithm is introduced, and the limitations in Doppler centroid ambiguity and motion parameter derivation are studied.

2.1 Introduction

Signal modeling and phase analyzing are the basis of SAR GMTI and GMTIm theories. Both the characters and processing problems of moving targets in real data can be explained by the signal model. Therefore, it is necessary to study on the signal model in the beginning of this book. After modeling the echo signal of a moving target, a detailed analysis of the impact of motion parameters on the echo phase in this chapter, and the different characters of moving targets with different motions, which are both the problems and clues of GMTI and GMTIm algorithms, are discussed.

In real applications, single-channel SAR systems still outnumber multi-channel SAR systems in China, due to the high expense and complex system structure of a multi-channel SAR system. In the signal processing point of view, the performances of multi-channel GMTI algorithms are higher due to the expense of complex system structures and algorithms. Although single-channel GMTI algorithms have been studied for years, there are many problems in real applications, considering the unknown and complex motions of moving targets. Compared with spaceborne SAR, airborne SAR has a lower speed and a higher resolution, which endows airborne SAR a lower detectable speed and a finer indication pixel. Therefore, this book mainly focuses on the single-channel GMTI and GMTIm algorithms of airborne SAR systems.

J. Yang, *Study on Ground Moving Target Indication and Imaging Technique of Airborne SAR*, Springer Theses, DOI 10.1007/978-981-10-3075-8_2

In this chapter, the signal model of a moving target is established, and the principles of several traditional single-channel GMTI and GMTIm algorithms are introduced, which is organized as follows. In Sect. 2.2, the principle of a SAR system is briefly introduced, and the signal model of a stationary target is established. In Sect. 2.3, the signal model of a moving target is established, and the relationship between the echo property and the motions is deeply analyzed. In Sects. 2.4 and 2.5, traditional single-channel SAR GMTI and GMTIm algorithms are presented respectively, and their limitations are discussed. Finally, conclusive remarks are provided in Sect. 2.6.

2.2 Principle of SAR

SAR is an advanced 2-D high resolution radar, which is able to acquire high imaging resolutions in both the range and azimuth directions. For a real aperture radar, the azimuth resolution relies on both the size of the aperture and the range: bigger aperture and shorter range make higher azimuth resolution. Therefore, in order to improve the azimuth resolution, the aperture size must be enlarged. The innovation of SAR is to simulate an equivalent large azimuth aperture by moving the radar in the azimuth direction with a constant velocity. On the other hand, the high range resolution of SAR is obtained by transmitting and receiving a wide-band linear modulated (LFM) signal.

During the azimuth time t_a, the platform flies from O to O_1 with a constant velocity V_a. R_0 and $R(t_a)$ represent the nearest and instantaneous slant ranges between the platform and the target P, respectively. H and X represent the height of the platform and the flat range, respectively. According to Fig. 2.1, $R(t_a)$ can be expressed as

$$R(t_a) = \sqrt{R_0^2 + (V_a t_a)^2} \tag{2.2.1}$$

Expand Eq. 2.2.1 into a Taylor series and keep it to the second-order term of t_a, then Eq. 2.2.1 can be approximated as

$$R(t_a) \approx R_0 + \frac{V_a^2}{2R_0} t_a^2 \tag{2.2.2}$$

Suppose the transmitted signal is a LFM signal with a carrier frequency f_0, a modulation rate K_r and a pulse band-width T_r, then the transmitted signal $s_t(t_r)$ can be expressed as

$$s_t(t_r) = rect\left(\frac{t_r}{T_r}\right) \exp\left[j2\pi\left(f_0 t_r + \frac{K_r}{2} t_r^2\right)\right] \tag{2.2.3}$$

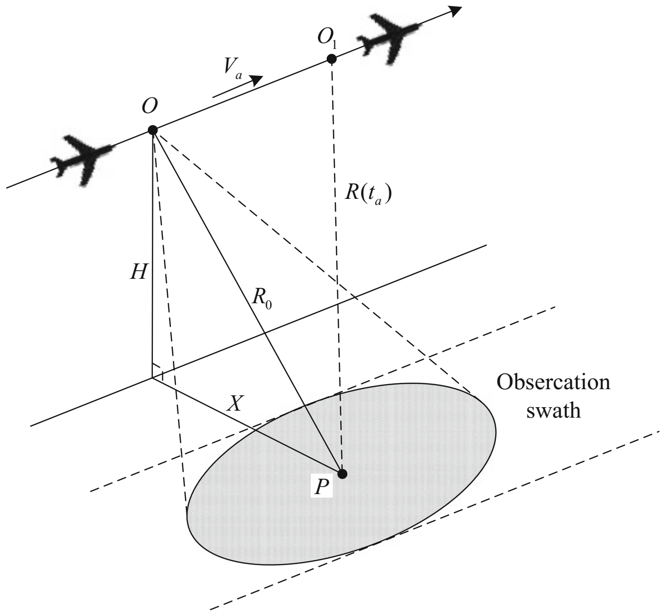

Fig. 2.1 Broadside geometry of a stationary target in airborne SAR

where $rect(\cdot)$ represents the rectangle window of the transmitted signal, and t_r denotes the range time. After the range compression, the echo signal of target P can be expressed as

$$s_r(t_a, t_r) = A_0\omega_a(t_a)\sin c\left[\pi B_r\left(t_r - \frac{2R(t_a)}{c}\right)\right]\exp\left[-j\frac{4\pi}{\lambda}R(t_a)\right] \tag{2.2.4}$$

where A_0 is the complex reflection coefficient of the moving target, B_r and λ are the bandwidth and wavelength of the transmitted signal, respectively, and c is the speed of light.

From Eq. 2.2.4, the range phase information is contained in the sinc function, which indicates that the range phase is related to the instantaneous slant range $R(t_a)$. The azimuth phase information is contained in the exponential terms, which means that it is also related to $R(t_a)$. Substitute Eq. 2.2.2 into Eq. 2.2.4, it yields

$$\begin{aligned} s_r(t_a, t_r) = & A_0\omega_a(t_a)\sin c\left[\pi B_r\left(t_r - \frac{2R_0}{c}\right)\right]\exp\left(-\mathrm{j}\frac{4\pi}{\lambda}R_0\right)\exp\left(-\mathrm{j}\frac{4\pi}{\lambda}\frac{V_a^2}{2R_0}t_a^2\right) \\ & \cdot\exp\left(-\mathrm{j}\frac{4\pi K_r}{\mathrm{c}}\frac{V_a^2}{2R_0}t_r t_a^2\right) \end{aligned} \tag{2.2.5}$$

In Eq. 2.2.5, the first exponential term denotes the range location of the target; the second exponential term represents the azimuth phase of the target. It can be noted that the azimuth phase of a point target in stripmap SAR is a second-order function of t_a, which makes it a LFM signal with an azimuth modulation rate f_{dr} as

$$f_{dr} = \frac{2V_a^2}{\lambda R_0} \tag{2.2.6}$$

Therefore, the azimuth compression can be achieved by utilizing a matched filter with modulation rate f_{dr}. If the modulation rate of the matched filter is mismatched, the second-order azimuth phase cannot be accurately compensated, and the azimuth dispersion is induced.

The third exponential term of Eq. 2.2.5 represents the RCM of the target. The RCM contains the range curve migration and the RWM. In broadside stripmap SAR, there is only the range curve migration with the absence of the squint angle. The RCM error will cause an energy dispersion of a target among multiple range cells if not accurately compensated.

According to the analysis above, the core of SAR signal processing is to compensate the phase errors of both the range and azimuth directions. The range and azimuth phase errors are compensated by using the matched filters. Since the transmitted signal is known, the range matched filter is mostly accurate. The azimuth matched filter is calculated and estimated, so it may induce azimuth phase errors if the matched filter is not accurate. The first-order azimuth phase error will cause the dislocation of the target; the second-order azimuth phase error will cause the broadening of the main-lobe; the third-order azimuth phase error will cause the asymmetry of the side-lobes; the fourth-order azimuth phase error will cause the raise of the side-lobes. RCMC is also an important part. Different algorithms have different ways to accomplish the RCMC.

As to a moving target, the signal form is the same as that of a stationary target, while the phase information is different with the existence of the motion. Therefore, the imaging algorithms that suit the stationary target processing are also suitable for the moving targets, if only the imaging parameters are accurately estimated.

2.3 Signal Analysis of Moving Target in SAR

2.3.1 Signal Model of a Moving Target

In a typical airborne SAR system, the synthetic aperture time is several seconds. During the synthetic aperture time, a target is radiated and reflected the microwave continuously. In most articles, the moving target is assumed to be moving with a constant velocity or a constant acceleration during the synthetic aperture time. According to this assumption, A broadside SAR configuration with a moving target in the slant range domain is shown in Fig. 2.2.

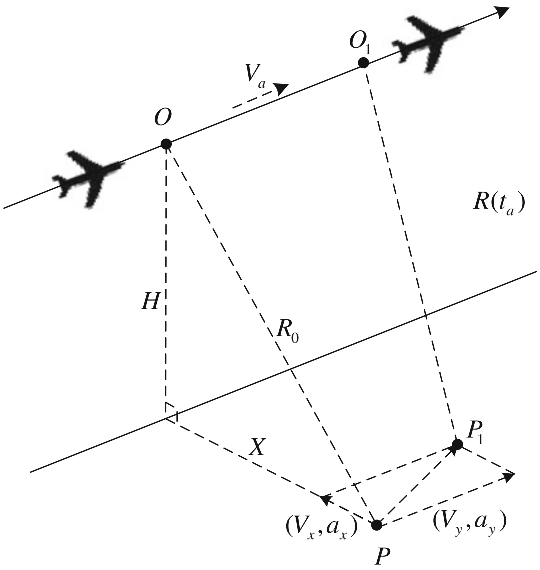

Fig. 2.2 Broadside geometry of a moving target in a single-antenna SAR system

The platform parameters are the same as in Fig. 2.1, whereas the target is a moving target with cross-track velocity V_x, cross-track acceleration a_x, along-track velocity V_y and along-track acceleration a_y. During the azimuth time t_a, the platform flies from O to O_1 with a constant velocity V_a, while the moving target moves from P to P_1. Therefore, the instantaneous slant range $R(t_a)$ can be expressed as

$$R(t_a) = \sqrt{H^2 + \left(X - V_x t_a - \frac{1}{2} a_x t_a^2\right)^2 + \left(V_a t_a - V_y t_a - \frac{1}{2} a_y t_a^2\right)^2} \qquad (2.3.1)$$

Expand Eq. 2.3.1 into a Taylor series and keep it to the second-order term of t_a, then Eq. 2.3.1 can be approximated as

$$R(t_a) \approx R_0 - \frac{X}{R_0} V_x t_a + \frac{(V_a - V_y)^2 - a_x X}{2R_0} t_a^2 \qquad (2.3.2)$$

The relationship of the motion parameters between the slant range domain and range domain can be expressed as

$$\frac{X}{R_0} = \frac{V_r}{V_x} = \frac{a_r}{a_x} \qquad (2.3.3)$$

where V_r and a_r represent cross-track velocity and acceleration in the slant-range domain respectively as shown in Fig. 2.3. Substitute Eq. 2.3.3 into Eq. 2.3.2, it yields

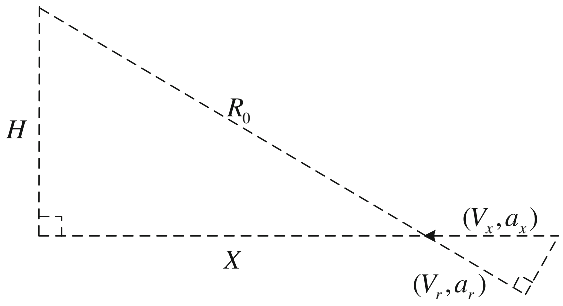

Fig. 2.3 Projection relationship between the range and slant-range domain

$$R(t_a) \approx R_0 - V_r t_a + \frac{(V_a - V_y)^2 - a_r R_0}{2R_0} t_a^2 \tag{2.3.4}$$

Substitute Eq. 2.3.4 into Eq. 2.2.4, the echo signal of the moving target can be expressed as

$$\begin{aligned} s_r(t_a, t_r) = {} & A_0 \omega_a(t_a) \sin c\left[\pi B_r\left(t_r - \frac{2R_0}{\mathrm{c}}\right)\right] \exp\left(\mathrm{j}\frac{4\pi}{\lambda} V_r t_a\right) \exp\left(-\mathrm{j}\frac{4\pi}{\lambda}\frac{(V_a - V_y)^2 - R_0 a_r}{2R_0} t_a^2\right) \\ & \cdot \exp\left(\mathrm{j}\frac{4\pi K_r}{\mathrm{c}} V_r t_r t_a\right) \exp\left(-\mathrm{j}\frac{4\pi K_r}{\mathrm{c}}\frac{(V_a - V_y)^2 - R_0 a_r}{2R_0} t_r t_a^2\right) \exp\left(-\mathrm{j}\frac{4\pi}{\lambda} R_0\right) \end{aligned} \tag{2.3.5}$$

Compare Eq. 2.3.5 with Eq. 2.2.5, it is noted that the signal model of the moving target is different from that of a stationary target. The first exponential term of Eq. 2.3.5 is the Doppler centroid phase, which results in the azimuth dis-location of the moving target. The second exponential term is the second-order azimuth phase, it is also different from a stationary target, indicating that the Doppler modulation rate of a moving target differs from that of a stationary target. The third and fourth exponential terms are the RCM of the moving target. Compared with a stationary target, an additional RWM is induced by the motions, and the range curve migration is different from a stationary target. The RCM will deteriorate the imaging resolution if not accurately compensated, which is also a reason why a moving target appears smeared in a stationary SAR image. The Doppler parameters of a moving target can be represented as

$$f_{dc} = \frac{2V_r}{\lambda} \tag{2.3.6a}$$

$$f_{dr} = \frac{2\left[(V_a - V_y)^2 - R_0 a_r\right]}{\lambda R_0} \tag{2.3.6b}$$

$$H_{rwm} = \exp\left(\mathrm{j}\frac{4\pi K_r}{\mathrm{c}} V_r t_r t_a\right) \tag{2.3.6c}$$

$$H_{rcm} = \exp\left(-\mathrm{j}\frac{4\pi K_r}{\mathrm{c}} \frac{(V_a - V_y)^2 - R_0 a_r}{2R_0} t_r t_a^2\right) \tag{2.3.6d}$$

where f_{dc} represents the Doppler centroid, H_{rwm} and H_{rcm} represent RWM and RCM, respectively.

From Eqs. 2.3.6a, 2.3.6b, 2.3.6c, 2.3.6d it can be noted that Doppler centroid and RWM are impacted by the cross-track velocity of a moving target, whereas the Doppler modulation rate and RCM is affected by both the along-track velocity and the cross-track acceleration.

Therefore, the Doppler parameters of a moving target changes correspondingly with the motion parameters of the moving target. The relationship between the Doppler parameters and the motion parameters is the reason why a moving target appears smeared and dislocation in the image, and also the lead to indicate and focus a moving target. All moving target processing algorithms are based on one or several parameters in Eqs. 2.3.6a, 2.3.6b, 2.3.6c, 2.3.6d, thus the impact of each parameter is analyzed as follows.

2.3.2 Doppler Centroid

The cross-track velocity is the most interesting parameter of the moving target in GMTI applications. Therefore, in most existing algorithms, the moving target is classified according to the values of their cross-track velocities [1–3]. For example, if the moving target has a slow cross-track velocity that its spectrum is submerged by the clutter, it is defined as a slow moving target. However, when the Doppler centroid of the moving target exceeds the limit of PRF, the Doppler ambiguity is induced. The Doppler ambiguity exists when the cross-track velocity meets the condition

$$V_x \geq \frac{\lambda \cdot PRF}{2} \tag{2.3.7}$$

In that case, the "fast" or "slow" cross-track velocity [4] cannot accurately reflect the spectrum character of the moving target. In the existence of the Doppler ambiguity, the moving targets can be classified according to the locations of their spectra. We classify the moving targets into three types, as shown in Fig. 2.4.

The red and black triangles in Fig. 2.4 represent the Doppler spectra of the moving target and the clutter, respectively. The spectra of the moving targets of Type I are completely located out of the clutter. Hence, a high-pass filter is able to separate the moving target from the clutter. In Type II, partial spectra of the moving

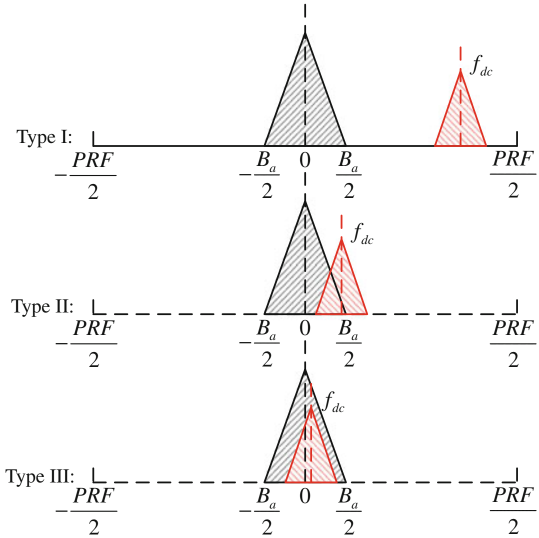

Fig. 2.4 Illustration of the three types of moving targets in the range-Doppler domain

target are submerged by the clutter. Type III represents the moving targets that are completely submerged by the clutter. The targets with slow cross-track velocities and the targets with fast cross-track velocities that aliased into the baseband, belong to Type III. In addition, given that the along-track velocity has no relationship with the Doppler centroid, the along-track moving targets also belong to Type III. The velocity information of the moving targets for each type is illustrated in Table 2.1, where B_a and B_m denote the Doppler bandwidths of the clutter and the moving target, respectively, and k is the number of the Doppler ambiguity.

In a whole synthetic aperture, the number of azimuth samples $N_a = PRF \cdot T_a$, where T_a represents the synthetic aperture time. Thus the number of azimuth dislocation samples can be calculated as

$$\Delta N = f_{dc}/PRF \cdot N_a \tag{2.3.8}$$

The synthetic aperture time $T_a = \frac{\lambda R_0}{L_a V_a}$, where L_a is the azimuth aperture size. Substitute it into Eq. 2.3.8, it yields that

$$\Delta N = \frac{2V_r R_0}{L_a V_a} \tag{2.3.9}$$

Table 2.1 Classification of moving targets

Type I	$\frac{B_a+B_m}{2} + k \cdot PRF < \left\lvert\frac{2V_r}{\lambda}\right\rvert < \frac{PRF}{2} + k \cdot PRF$
Type II	$\frac{B_a-B_m}{2} + k \cdot PRF < \left\lvert\frac{2V_r}{\lambda}\right\rvert < \frac{B_a+B_m}{2} + k \cdot PRF$
Type III	$k \cdot PRF \le \left\lvert\frac{2V_r}{\lambda}\right\rvert < \frac{B_a-B_m}{2} + k \cdot PRF$

Substitute azimuth sample interval $d_a = \frac{L_a}{2}$ into Eq. 2.3.9, the azimuth dislocation is

$$\Delta R = \frac{V_r}{V_a} R_0 \tag{2.3.10}$$

According to Eq. 2.3.10, the azimuth dislocation of a moving target is determined by its cross-track velocity.

2.3.3 Doppler Modulation Rate

According to Eq. 2.3.6b, the Doppler modulation rate of a moving target is related to the along-track velocity and cross-track acceleration. The Doppler modulation rates of a moving target and a stationary target differ in the existence of these two motion parameters. The change of the Doppler modulation rate can be expressed as

$$\Delta f_{dr} = \frac{2V_a^2}{\lambda R_0} - \frac{2\left[(V_a - V_y)^2 - R_0 a_r\right]}{\lambda R_0} = \frac{2\left[V_y(2V_a - V_y) + R_0 a_r\right]}{\lambda R_0} \tag{2.3.11}$$

The Doppler modulation rate directly affects the azimuth focusing performance. In the existence of Δf_{dr}, a moving target is smeared since there is the second-order azimuth phase error. The second-order azimuth phase error will lead to the main-lobe broaden, the peak declination of the main-lobe and peak rise of the side-lobes. The second-order azimuth phase error of a moving target in a stationary SAR image can be expressed as

$$\Delta\phi_a = \exp\left\{ j\frac{2\pi}{\lambda R_0}[V_y(2V_a - V_y) + R_0 a_r]t_a^2 \right\} \tag{2.3.12}$$

Equation 2.3.12 reaches its largest value at the edge of the synthetic aperture, therefore the maximum value of the second-order azimuth phase error is

$$\Delta\varphi_a = \frac{\pi}{2\lambda R_0}\left[V_y(2V_a - V_y) + R_0 a_r\right]T_a^2 \tag{2.3.13}$$

By using the typical airborne and spaceborne SAR system parameters as shown in Table 2.2 [5], the numerical second-order phase error can be calculated. Suppose the along-track velocity of a moving target is 10 m/s and the cross-track acceleration is 0.1 m/s^2, the second-order azimuth phase error is 149.43 rad in the airborne SAR situation, while the value is 3.013 rad in the spaceborne situation. An airborne SAR has a smaller velocity and nearer range length, and has a higher resolution. Therefore, the defocus of a moving target is more obvious in an airborne SAR image than in a spaceborne SAR image.

Table 2.2 Typical system parameters in airborne and spaceborne SAR

Platform	System parameters					
	Wavelength (m)	Range (km)	Platform velocity (m/s)	Synthetic aperture time (S)	Azimuth resolution (m)	Range resolution (m)
Airborne	0.032	850	7100	3.4	0.5	1.25
Spaceborne	0.057	30	250	0.64	5	6.25

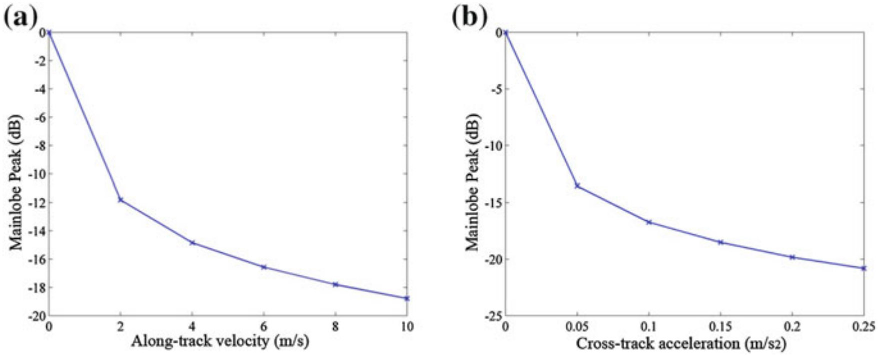

Fig. 2.5 Peak changes of the mainlobe with motions. **a** Changes with along-track velocity. **b** Changes with cross-track velocity

According to the analysis above, airborne SAR moving target imaging is a far more complicate issue than spaceborne SAR. Since the second-order azimuth error also causes the peak declination of the main-lobe, the moving target indication performance will be affected by using CFAR technique. By using the system parameters in Table 2.2, a set of simulations is operated, as shown in Fig. 2.5.

In Fig. 2.5a, the horizontal ordinate denotes the along-track velocity, which is 2, 4, 6, 8, 10 m/s; the vertical ordinate denotes the peak of the mainlobe, which is measured by dB. It can be noted that the peak of the mainlobe decreases with the increase of the along-track velocity. Figure 2.5b illustrates the relationship between the peak of the mainlobe and the cross-track acceleration. The cross-track accelerations are valued as 0.05, 0.1, 0.15, 0.2 and 0.25 m/s^2. It can be noted that the peak of the main-lobe also decreases with the increase of the cross-track acceleration. Therefore, it is proved that the change of Doppler modulation rate results in the smear of the image.

2.3.4 RCM

RCM is a phase error induced by the long synthetic aperture time. RCM reflects the changes of the instantaneous slant range, and exists in both the stationary and moving targets. The existence of RCM will lead to the energy of the target smear among multiple range gates, and will severely deteriorate the imaging quality.

According to the last exponential term of Eq. 2.2.5, in a broadside airborne SAR system, only the range curve migration exists. Thus, for the stationary target that locates at the center of the scene, its range curve migration reaches its largest value at the edge of the synthetic aperture. The largest range curvature can be expressed as

$$S_{rcm} = \frac{V_a^2}{2R_0}\left(\frac{T_a}{2}\right)^2 \tag{2.3.14}$$

Equations 2.3.6c and 2.3.6d are the RCM of a moving target. It can be noted that an additional RWM is induced by the cross-track velocity of the moving target, and the range curvature of a moving target is different from that of a stationary target. The range walk and curve migration of a moving target are expressed respectively as

$$S_{rwm} = V_r \frac{T_a}{2} \tag{2.3.15a}$$

$$S_{rcm} = \frac{(V_a - V_y)^2 - a_r R_0}{2R_0}\left(\frac{T_a}{2}\right)^2 \tag{2.3.15b}$$

The changes of RCM can be expressed as

$$\Delta S_{rwm} = V_r \frac{T_a}{2} \tag{2.3.16a}$$

$$\Delta S_{rcm} = \frac{2V_a V_y - V_y^2 + a_r R_0}{2R_0}\left(\frac{T_a}{2}\right)^2 \tag{2.3.16b}$$

According to the system parameters in Table 2.2, the values of Eq. 2.3.14 to Eqs. 2.3.15a, 2.3.15b can be calculated. Suppose the cross-track velocity of the moving target is 10 m/s, the cross-track acceleration is 0.1 m/s^2, and the along-track velocity is 10 m/s, in an airborne SAR situation, the range walk and curve migration of the moving target is 17 and 2.6299 m, and the range curve change is 0.3805 m. Compared with the range resolution 1.25 m, the RCM is far larger than the range resolution, which has to be corrected during imaging.

However, in the spaceborne SAR situation, the RCM of a stationary target is 3.0365 m, and the range walk and curve migration of the moving target is 3.2 and 3.0228 m. Compared with the range resolution 6.25 m, the RCM of the moving target is small, and the image resolution will not be significantly affected by the RCM of the moving target.

In conclusion, the RCM is much more severer in an airborne SAR system than in a spaceborne SAR system. Since the RCM is related to the motion parameters of a moving target, it is a very important parameter in GMTI and GMTIm algorithms.

2.4 Principle of Existing GMTI Algorithms

All existing GMTI algorithms use the Doppler characters of moving targets and their differences from those of the stationary targets to accomplish the target detection. There are mainly two parts in GMTI algorithms: clutter suppression and CFAR detection.

2.4.1 Principle of Single-Antenna GMTI Algorithms

Different GMTI algorithms use different methods to suppress the clutter. By suppressing the clutter, the spectra of moving targets can be separated from the clutter, and the SCR is increased.

(a) Spectrum filtering algorithm

According to the analysis in Sect. 2.3.2, a Doppler centroid shift is induced by the cross-track velocity of a moving target. The spectrum of the moving target will move towards the high-band of the PRF with the increase of the cross-track velocity, and the spectrum of the target will be eventually located outside the clutter. Based on the Doppler centroid shift, the moving target can be detected by setting up a series of band-pass filter in the high-band of PRF. Spectrum within the band-pass filter will be restrained, and the clutter will be suppressed. After the clutter suppression, the spectrum of the moving target can be extracted, and the target can be re-focused, as shown in Fig. 2.6.

In Fig. 2.6, n band-pass filters with different frequency center are set in the range-Doppler domain, and the clutter is not located within the band-pass filters. If the target has only the cross-track velocity, the target can be focused after shifting its spectrum into baseband. The flowchart of spectrum filtering algorithm is illustrated in Fig. 2.7.

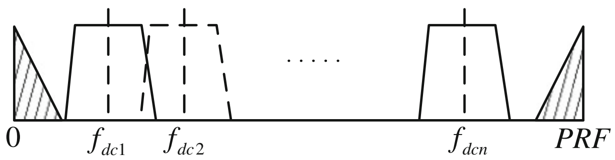

Fig. 2.6 Principle of the spectrum filtering algorithm

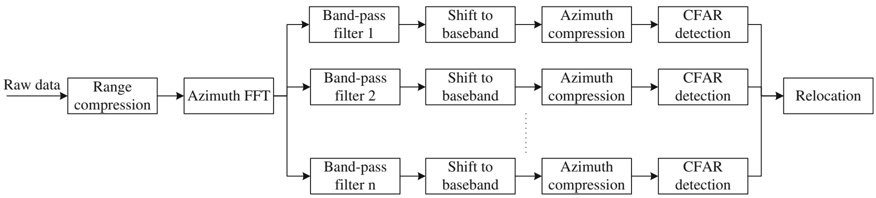

Fig. 2.7 Flowchart of the spectrum filtering algorithm

However, the spectrum filtering algorithm requires that the cross-track velocity of the moving target will not induce significant RCM, i.e., the RCM of the target must be less than half of the range resolution.

$$\left|\frac{V_r}{V_a}\right| < \frac{1}{\beta}\frac{\rho_r}{2R_0} \tag{2.4.1}$$

where β is the beam angle, ρ_r denotes the range resolution.

Moreover, the spectrum filtering algorithm requires that there is no Doppler ambiguity. The cross-track velocity has to satisfy the condition that

$$\frac{1}{2}\mu\beta < \left|\frac{V_r}{V_a}\right| < \frac{\lambda \cdot PRF}{2V_a} - \frac{\beta}{2} \tag{2.4.2}$$

where μ is the coefficient of antenna and signal processing.

The Doppler ambiguity will be induced in most practical applications. However, although the spectrum filtering algorithm requires that no Doppler ambiguity exists, it can still suppress the clutter only if the spectrum of the moving target locates outside the clutter.

In conclusion, there are mainly three limitations of spectrum filtering algorithm: first, the velocity detection range has a inconsistent requirement with the observation swath; second, the spectrum filtering algorithm cannot detect targets with slow cross-track velocity and blind velocity; third, targets with only along-track velocities cannot be detected.

(b) RDM algorithm

RDM algorithm is a representative algorithm that detects moving targets with the Doppler modulation rate change. It is firstly invented as a motion compensation algorithm that corrects the motion error of the platform during the flight. J.R. Moreira first applied this algorithm in GMTI, the principle of RDM algorithm is: The change of Doppler modulation rate can be detected by the relationship between neighboring Doppler power spectra. The moving target can be indicated by its Doppler centroid, and the along-track velocity and cross-track acceleration can be estimated.

There are mainly three limitations of RDM algorithm: first, only targets with the along-track velocity and cross-track acceleration can be detected, but the target with only the cross-track velocity cannot be detected; second, RDM algorithm is not effective for the detection of multiple targets which are located nearby; third, the Doppler parameter estimation precision is not high, and two motion parameters cannot be derived from one Doppler parameter.

Shear average algorithm also uses the Doppler modulation rate to detect moving targets. This algorithm uses the contrast ratio of sub-images focused with different Doppler modulated rates to judge whether there is a moving target in the sub-image. Moreover, shear average algorithm has also the disadvantages same as RDM algorithm.

(c) Time-frequency analysis algorithm

The signal character differences between a moving target and a stationary target can be revealed in the time-frequency domain. Motions of a moving target changes the Doppler centroid and Doppler modulation rate of the moving target, and time-frequency analysis algorithms are highly efficient in extracting the motion parameters. WVD transform is proposed by S. Barbarossa to extract and estimate the motion parameters of moving targets. After WVD transform, the azimuth spectrum is transformed into a straight line, the slope of the line is the Doppler modulation rate, and the frequency initial is the Doppler centroid. Suppose the signal is $s(t)$, the definition of WVD transform is

$$W(t,f) = \int s\left(t + \frac{\tau}{2}\right) s^*\left(t - \frac{\tau}{2}\right) \exp(-j2\pi\tau f) d\tau \tag{2.4.3}$$

The WVD transform has a poor performance in the low SNR condition, so the clutter suppression and spectrum extraction must be performed before WVD. Thus, WVD transform is more suited as a GMTIm algorithm but not a GMTI algorithm.

Furthermore, WVD transform is a bilinear transform, and is not suitable for multi-target detection and parameter estimation. Improved WVD transforms have been studied, while the performances are not promising as well. Wavelet transform is also a sort of new time-frequency analysis algorithms, but it has a heavy calculation burden and not suited for practical applications.

2.4.2 CFAR Detection

CFAR detection is a classical technique of radar detection. In a radar system, if the detection threshold V_T is set as a constant value, the false-alarm rate P_{fa} will rise with the increase of interference σ:

$$P_{fa} = \exp\left(-\frac{V_T^2}{2\sigma^2}\right) \tag{2.4.4}$$

In a radar system, there are not only the thermal noise within the receiver, but also the interferences from the clutter and the enemy. These interferences are strong in most situations, and their amplitudes vary in different scenes. In that case, the false-alarm rate will not be constant any more. The method to keep a constant false-alarm rate is called CFAR detection [6].

With the development of radar detection, many CFAR detection methods are invented [7–13]. In practical applications, the specific method must be chosen according to the echo distribution. In a low-resolution SAR system, the amplitude of the echo obeys the Rayleigh distribution, while the amplitude of the echo obeys other distributions such as Swerling model [14], lognormal model [15] and χ^2 distribution. In most SAR data, the Rayleigh distribution assumption is convincing, so the classical CA-CFAR algorithm in Rayleigh distribution is introduced in this section.

Suppose the probability distribution function of clutter y is expressed as

$$p(y) = \frac{y}{\sigma^2}\exp\left(-\frac{y^2}{2\sigma^2}\right) \tag{2.4.5}$$

Let $x = \frac{y}{\sigma}$, $V_0 = \frac{V_T}{\sigma}$, and substitute them into Eq. 2.4.4, it yields

$$P_{fa} = \exp\left(-\frac{V_0^2}{2}\right) \tag{2.4.6}$$

For the new clutter, the false-alarm rate follows Eq. 2.4.6, which is not related to the clutter. The relationship between the derivation σ and the mean μ is

$$\sigma = \sqrt{\frac{2}{\pi}}\mu \tag{2.4.7}$$

The principle of CA-CFAR is illustrated in Fig. 2.8.

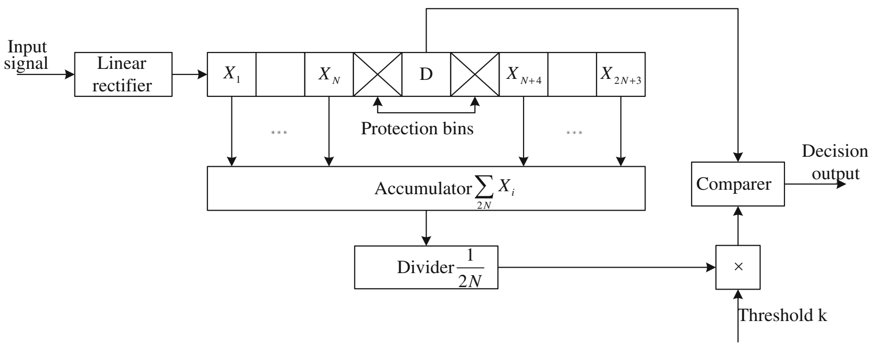

Fig. 2.8 Principle of CA-CFAR detection

2.5 Principle of GMTIm Algorithms

After GMTI, the echoes of moving targets are separated from that of the clutter. GMTIm algorithms are used to focus and relocated the moving target by estimating its Doppler parameters. The main operations of GMTIm algorithms contain RCMC and Doppler parameter estimation.

2.5.1 *RCMC of Moving Targets*

The RCM of the moving target must be accurately corrected so as to get a focused image of the target. However, the RCM of the moving target is different from that of the clutter, and is unknown without the information of motion parameters. In most articles, the RCMC of moving targets is performed by using the Keystone transform [16].

Before the range compression, the echo of a point target in a broadside airborne SAR can be expressed as

$$s_r(t_a,t_r) = A_0\omega_a(t_a)rect\left[\frac{t_r-\frac{2R(t_a)}{c}}{T_r}\right]\exp\left(j\pi K_r\left(t_r-\frac{2R(t_a)}{c}\right)^2\right)\exp\left(-j\frac{4\pi f_c}{c}R(t_a)\right) \tag{2.5.1}$$

where T_r denotes the pulse duration, f_c denotes the carrier frequency. Transform Eq. 2.5.1 into range-frequency domain, it yields

$$s_r(t_a,f_r) = A_0\omega_a(t_a)rect\left[\frac{f_r}{K_rT_r}\right]\exp\left(-j\pi\frac{f_r^2}{K_r}\right)\exp\left(-j\frac{4\pi(f_c+f_r)}{c}R(t_a)\right) \tag{2.5.2}$$

where f_r is the range frequency. In Eq. 2.5.2, the first exponential term can be compensated by a range matched filter or the deramping operation so as to accomplish the range compression. The RCM and azimuth phase information are hidden in the second exponential term. Suppose it is represented by $\Phi(t_a,f_r)$, substitute Eq. 2.3.4 into Eq. 2.5.2, it yields

$$\begin{aligned}\Phi(t_a,f_r) = {} & \exp\left(-j\frac{4\pi(f_c+f_r)}{c}R_0\right)\exp\left(j\frac{4\pi V_r}{c}(f_c+f_r)t_a\right)\\ & \cdot\exp\left(-j\frac{2\pi\left((V_a-V_y)^2-a_rR_0\right)}{cR_0}(f_c+f_r)t_a^2\right)\end{aligned} \tag{2.5.3}$$

In Eq. 2.5.3, the second exponential term contains the Doppler centroid shift and the RWM; the third exponential term contains the second-order azimuth phase error and the range curve migration. It is noted that the coupling of the range-frequency and azimuth-time denotes the RWM, and the coupling of the range-frequency and the second-order azimuth-time denotes the range curve migration. Transform the azimuth time t_a by

$$t_a = \frac{f_c}{f_c + f_r}\tau_a \tag{2.5.4}$$

Substitute it into Eq. 2.5.3, it yields

$$\begin{aligned}\Phi(t_a, f_r) = {} & \exp\left(-j\frac{4\pi(f_c + f_r)}{c}R_0\right)\exp\left(j\frac{4\pi V_r}{c}f_c\tau_a\right) \\ & \cdot \exp\left(-j\frac{2\pi\left((V_a - V_y)^2 - a_r R_0\right)}{cR_0}\frac{f_c^2}{f_c + f_r}\tau_a^2\right)\end{aligned} \tag{2.5.5}$$

It is noted that the range-frequency and azimuth-time is decoupled after the transform, and in turn the RWM is corrected. Equation 2.5.4 is the definition of Keystone transform [17–19]. By using the Keystone transform, the RWM can be corrected without the estimation of the cross-track velocity V_r.

It is also noted from Eq. 2.5.5 that the range curve migration is not corrected by using the Keystone transform. Thus, researchers proposed the second-order Keystone transform [20], which is defined as

$$t_a = \left(\frac{f_c}{f_c + f_r}\right)^{\frac{1}{2}}\tau_a \tag{2.5.6}$$

Substitute Eq. 2.5.6 into Eq. 2.5.3, it yields

$$\begin{aligned}\Phi(t_a, f_r) = {} & \exp\left(-j\frac{4\pi(f_c + f_r)}{c}R_0\right)\exp\left(j\frac{4\pi V_r}{c}f_c^{\frac{1}{2}}(f_c + f_r)^{\frac{1}{2}}\tau_a\right) \\ & \cdot \exp\left(-j\frac{2\pi\left((V_a - V_y)^2 - a_r R_0\right)}{cR_0}f_c\tau_a^2\right)\end{aligned} \tag{2.5.7}$$

It can be noted that the range curve migration is corrected after the second-order Keystone transform, and half of the RWM is removed. In the moving target imaging of an airborne SAR system, the impact of the RWM on the imaging quality of a moving target is far severer than the range curve migration [21], so the first-order Keystone transform is the most widely-used algorithm in RCMC of moving targets, and the second-order Keystone transform is only suited for the imaging of along-track moving targets.

Since the azimuth time is a discrete value, the Keystone transform is accomplished by sinc interpolation. The precision of sinc interpolation is highly related to the length of the interpolation core, and long interpolation core requires heavy calculation burden. Therefore, Keystone transform is not suitable for real-time processing.

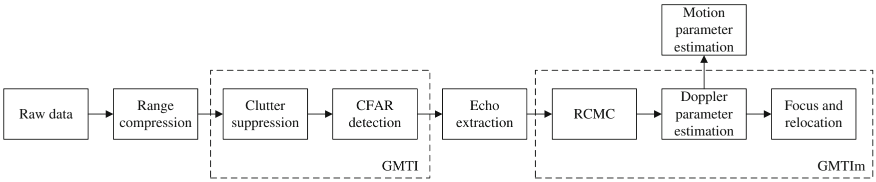

Fig. 2.9 Flowchart of GMTI and GMTIm in airborne SAR

Another disadvantage of Keystone transform is that it is only effective without the existence of Doppler centroid ambiguity. If there is Doppler centroid ambiguity in the echo, the Doppler centroid ambiguity number must be estimated before Keystone transform.

2.5.2 Motion Parameter Estimation

After RCMC, the energy of the moving target is concentrated into a range gate, and the echo of the moving target can be viewed as a 1-D signal. The Doppler parameters are estimated from the azimuth signal, and the target can be focused and relocated using the estimations.

Since the azimuth signal of the target in SAR can be viewed as a chirp signal, the Doppler parameters can be accurately estimated using the time-frequency analysis algorithms, such as WVD transform, FrFT [22], wavelet transform and so forth.

After the Doppler parameter estimation, motion parameters can be derived. The cross-track velocity can be calculated as

$$\hat{V}_r = \frac{\lambda \hat{f}_{dc}}{2} \tag{2.5.8}$$

Since the two motion parameters cannot be derived from one Doppler parameter, the cross-track acceleration and the along-track velocity cannot be derived from the Doppler modulation rate at the same time. Thus, the acceleration is neglected in practical applications. The along-track velocity is calculated as

$$\widehat{V}_y = V_a - \sqrt{\frac{\lambda R_0 \hat{f}_{dr}}{2}} \tag{2.5.9}$$

If there are multiple moving targets in the scene, each target must be estimated and focused independently. The flowchart of the whole moving target processing is illustrated in Fig. 2.9.

2.6 Conclusion

The principle of SAR imaging has been briefly introduced in this chapter, and the echo signals of stationary and moving targets in a broadside airborne SAR system have been established. By comparing the Doppler parameters between the stationary and moving targets, the relationship between motion parameters of moving targets and the Doppler centroid, Doppler modulation rate and RCM has been analyzed.

Based on the analysis, three classical single-channel GMTI algorithms have been introduced in this chapter, and their limitations have been discussed. Moreover, the principle of GMTIm algorithms with Keystone transform and time-frequency analysis algorithm has been introduced, and the limitations in Doppler centroid ambiguity and motion parameter derivation have been studied.

The content in this chapter is the foundation of the following chapters. The limitations of existing algorithms mentioned in this chapter are further studied and solved in the proposed algorithms in this book.

References

1. Qian J, Lv X, Xing M et al (2010) Parameter estimation of the fast moving target based on tri-channel airborne SAR-GMTI. J Xidian Univ 37(2):235–241
2. Dai D, Liu J, Tang H et al (2005) Slowly moving target detection and imaging using single-antenna SAR. Sig Process 21(4A):550–554
3. Zhu S, Liao G, Zhou Z et al (2009) Approach to ground slowly moving target parameter-estimation for airborne dual-channel SAR systems. Syst Eng Electron 31 (12):2848–2852
4. Zhao Y (2007) Ground moving target indication of synthetic aperture radar. Institute of Electronics, Chinese Academy of Sciences
5. Cumming IG, Wong FH (2005) Digital processing of synthetic aperture radar data: algorithms and implementation. Artech House, Norwood
6. Nitzberg R (1972) Constant-False-Alarm-Rate signal processors for several types of interference. IEEE Trans Aerosp Electron Syst 8(1):27–34
7. He Y, Guan J, Peng Y et al (1999) Radar target detection and CFAR technique. Tsinghua University Press, Beijing
8. Rohling H (1983) Radar CFAR thresholding in clutter and multiple target situations. IEEE Trans Aerosp Electron Syst 19(3):608–621
9. Ji S, Huangpu K, Zhou L et al (1990) A new constant-false-alarm-rate (CFAR) processor. J Nat Univ Defense Technol 12(4):116–121
10. Thomas JB (1970) Nonparametric detection. Proc IEEE 58(5):623–631
11. Guan J, He Y, Peng Y (2000) Study of distributed CFAR detection based on local test statistics and its fusion strategy. ACTA Electronica Sin 28(3):125–127
12. Cai LJ, Wang H (1994) Further results on adaptive filtering with embedded CFAR. IEEE Trans Aerosp Electron Syst 30(4):1009–1020
13. Wanielik G, Stock DJR (1990) Measured scattering-matrix-data and a polarimetric CFAR-detector which works on this data. In: IEEE international radar conference, Piscataway, NJ, USA, 1990, pp 514–519

14. Swerling P (1997) Radar probability of detection for some additional fluctuating target cases. IEEE Trans Aerosp Electron Syst 33(2):698–709
15. Trunk GV, George SF (1970) Detection of targets in non-Gaussian sea clutter. IEEE Trans Aerosp Electron Syst 6(5):620–628
16. Perry RP, Dipietro RC, Fante RL (1999) SAR imaging of moving targets. IEEE Trans Aerosp Electron Syst 35(1):188–200
17. Tang L, Li D, Wu Y et al (2005) Imaging of ground moving targets based on airborne SAR. Syst Eng Electron 27(10):1681–1684
18. Qian J, Su J, Li L et al (2010) Tri-channel SAR-GMTI high-speed target imaging and motion parameter estimation using KWT. J Electron Inf Technol 32(7):1660–1667
19. Yin J, Li D, Tang L et al (2007) Spaceborne SAR detecting and imaging of airborne moving targets. ACTA Electronica Sin 35(6):1032–1036
20. Zhou F, Li Y, Xing M et al (2007) An effective approach to ground moving target imaging and motion parameter estimation for single channel SAR system. ACTA Electronica Sin 35 (3):543–548
21. Yang J, Huang X, Jin T et al (2011) New approach for SAR imaging of ground moving targets based on a Keystone transform. IEEE Geosci Remote Sens Lett 8(4):829–833
22. Sun H, Liu G, Gu H et al (2002) Application of the fractional Fourier transform of moving target detection in airborne SAR. IEEE Trans Aerosp Electron Syst 38(4):1416–1424

Springer

http://www.springer.com/978-981-10-3074-1

Study on Ground Moving Target Indication and Imaging Technique of Airborne SAR
Yang, J.
2017, XX, 109 p. 57 illus., 27 illus. in color., Hardcover
ISBN: 978-981-10-3074-1